VOLUME 8 ISSUE 2 2022

ISSN 2454-3055

INTERNATIONAL JOURNAL OF ZOOLOGICAL INVESTIGATIONS

Forum for Biological and Environmental Sciences

Published by Saran Publications, India

International Journal of Zoological Investigations Vol. 8, No. 2, 587-604 (2022)

International Journal of Zoological Investigations
Contents available at Journals Home Page: www.ijzi.net
Editor-in-Chief: Prof. Ajai Kumar Srivastav
Published by: Saran Publications, Gorakhpur, India

ISSN: 2454-3055

Biosynthesis and Characterization of Iron Oxide Nanoparticles and their Antibacterial Activity

Venkadachalam E.[1], Indra V.[1]*, Abdul Rahim M.[1] and Pazhani P.[2]

[1]PG and Research Department of Zoology, Presidency College, Chennai - 05, Tamil Nadu, India
[2]Department of Zoology, Government Higher Secondary School, Vadamathimangalam, Thiruvannamalai 606907, Tamil Nadu, India

**Corresponding Author*

Received: 24th August, 2022; **Accepted:** 10th October, 2022; **Published online:** 19th October, 2022

https://doi.org/10.33745/ijzi.2022.v08i02.073

Abstract: The present investigation was aimed to develop an easy, low-cost and eco-friendly method for the synthesis of Chitosan based iron oxide Nanoparticles (Cs-FeNPs) using shells of *Penaeus monodon*. The synthesized Cs-FeNPs were characterized by using Ultraviolet-Visible spectroscopy (UV), Fourier-Transform Infrared spectroscopy (FT-IR), X-ray Diffraction (XRD), Transmission Electron Microscope (HR-TEM) and Scanning Electron Microscope (SEM with EDAX). The visible dark black color formation and surface plasmon resonance at 233 nm indicates the biosynthesis of Cs-FeNPs. The TEM images showed polydispersal, and spherical Cs-FeNPs particle size of 3 to 5 nm. Antibacterial activity of chitosan aqueous extract and Cs-FeNPs showed an excellent activity against Gram-positive bacteria (*Staphylococcus aureus* and *Enterococcus faecalis*) and Gram-negative bacteria (*Escherichia coli*, *Enterobacter, Klebsiella pneumoniae* and *Pseudomonas aeruginosa*).

Keywords: Nanoparticles, Chitosan, Cs-FeNPs, Chacterization, Antibacterial activity, *Staphylococcus aureus*, *Enterococcus faecalis*, *Escherichia coli, Enterobacter*, *Klebsiella pneumonia*, *Pseudomonas aeruginosa*, *Penaeus monodon*

Citation: Venkadachalam E., Indra V., Abdul Rahim M. and Pazhani P.: Biosynthesis and characterization of iron oxide nanoparticles and their antibacterial activity. Intern. J. Zool. Invest. 8(2): 587-604, 2022.

https://doi.org/10.33745/ijzi.2022.v08i02.073

Introduction

The synthesis of Nanoparticles (NPs) involves numerous physico-chemical, biological, and hybrid methods for integrating different types of NPs. The NPs formed by the use of each method exhibit specific properties. Whereas chemical synthesis methods may lead to detrimental effect on medical applications due to their toxicity. Therefore, the biological synthesis of NPs in animal extracts is currently becoming a boon for researchers. The synthesis of metal NPs using wastes animal tissues, animal extracts, exudates and other parts of living animals is a modern alternative to their

production. The use of eco-friendly materials like animal secondary metabolities for the synthesis of Cs-FeNPs offers more benefits in the pharmaceutical and other biomedical fields. Natural biosynthetic metal NPs are non-toxic and eco-friendly (Filser *et al*., 2013; Saif *et al*., 2016; Tamara *et al*., 2018; Plachtova *et al*., 2018; Abdallah *et al*., 2020; Azizi, 2020; Hernández-Hernández *et al*., 2020; Guo *et al*., 2020). Nanotechnology can be described as the control and manipulation of matter on the nanoscale level or dimension by using scientific knowledge of different biomedical and Industrial applications. Nanomaterials gained immense popularity in scientific and technological advancements due to their significant chemical, biological and physical properties and they can be produced with extreme magnetic, electrical, mechanical, optical, and catalytic properties when compared to their original counterparts (Nadeem Baig *et al.,* 2021).

Biological systems such as animals and microorganisms produce secondary metabolites, most of which are in nanoscale dimensions. Cellular extracts from these biological organisms are used to synthesize NPs of different sizes and chemical compositions. The eco-friendly assembly of metal NPs extracted from different sources of animals and microorganisms is the best process for packaging for the most affordable price. The components in animal extracts are responsible for reducing iron while the water-soluble heterocyclic components stabilize the formed NPs. Suitable precursors such as ferric chloride and ferrous sulphate can be used to reduce animal extracts. Thus eco-friendly NPs has attracted a lot of attention and involves a wide range of processes that reduce or eliminate toxins to restore the environment (Yarjanli *et al*., 2017; Arias *et al*., 2018; Shevtsov *et al*., 2018; Salimi *et al*., 2018).

Chitosan is known as deacetylated chitin, which is a natural polycationic linear polysaccharide derived from partial deacetylation of chitin. Chitin is the structural element present in the exoskeleton of insects, crustaceans and cell walls of fungi, and the second most abundant natural polysaccharide after cellulose (Moise *et al*., 2017; Patel *et al*., 2019).

The interesting characteristics of Chitosan such as biocompatibility, non-toxicity, low allergen city and biodegradability allowed it to be used in various scientific fields such as wound healing, wound dressing, larvicidal properties, and therapeutic agent for dry mouth syndrome, anticancer, antitumor, antimicrobial, vascular hemostasis, hypocholesterolemic effect, obesity, enhancer for mucosal immunity, euglycemic-hyperinsulinemic, trauma, drug delivery, angiogenesis, weight loss, limb bone defects, tissue engineering, atherosclerosis, cancer chemotherapy, tumor growth, metastasis, anti-aging property and antioxidant activities (Sreeja and Nair, 2018; Kim *et al*., 2019; Gaiani *et al*., 2019; Khan *et al*., 2019; Üzek *et al*., 2019; Katz, 2020).

Despite the great progress in antimicrobial agent development, many infectious diseases remain difficult to treat, due to a lot of reasons such as the emergence and spread of resistant clones, the lack of the antimicrobial structures and suboptimal pharmacological properties of the existent antimicrobial substances, which sometimes are difficult to reach active concentrations inside bacterial strains or around body sites. Chitosan, a promising biocompatible and biodegradable biopolymer show potential antimicrobial activity (Zheng, Zhu *et al.,* 2013). Nanocomposites synthesized from Chitosan may exhibit antimicrobial activity against various pathogens (Davoodbasha *et al.,* 2016). The present investigation was aimed to develop an easy, low-cost and eco-friendly method for the synthesis of Chitosan based iron oxide Nanoparticles (Cs-FeNPs) using shells of *Penaeus monodon*.

Materials and Methods

Collection and authentic identification of shrimp:

The tiger shrimps were collected from Kasimedu fish landing centre, Chennai, Tamil Nadu, India and were taxonomically identified as *Penaeus monodon* and authenticated by Dr. C. P. Balasubramanian,

Fig. 1: (A) *Penaeus monodon*, (B) dried shells of *Penaeus monodon* and (C) Crushed form of shell.

Principal Scientist and SIC CCD, CIBA, Chennai, Tamil Nadu, India.

Sample Preparation:

The Shells of *Penaeus monodon* were washed thoroughly with running tap water and finally rinsed with double distilled water. Then they were shade dried under room temperature for a week. After dried completely they were crushed and stored in the refrigerator as a stock for further usage (Fig. 1).

Extraction of shrimp shell waste (*Penaeus monodon*):

The crushed shells of *Penaeus monodon* were extracted by following three steps such as demineralization, deproteinization and deacetylation to obtain the byproduct called chitosan according to the method of Nadia *et al*. (2018).

Preparation of Chitosan aqueous extract:

The aqueous extract of the Chitosan was prepared by mixing 5 g of Chitosan powder in a 100 ml of Double Distilled Water (DDW) in 200 ml beaker. The solution was heated at 100°C in the water bath. The aqueous extract of chitosan was then collected and centrifuged at 10,000 rpm for 10 min to remove the suspended Chitosan particles. The centrifuged supernatant solution Chitosan aqueous extract was taken for the synthesis of iron oxide nanoparticles (Figs. 2A, B).

Synthesis of Cs-FeNPs:

Ferrous sulphate (0.1 ml of 0.1 M) and ferric chloride (0.1 ml of 0.1 M) solution was mixed with 100 ml of deionized water. To this solution 50 ml of Chitosan aqueous extract was added followed by the addition of 10 ml of NaOH (0.1 M) to the mixture and stirred at 50°C for 1 h. Nitrogen atmosphere was maintained to remove any dissolved oxygen present in the solution. After the formation of brown precipitate, the solution was further stirred for 1 h at 45°C. It is then centrifuged, the supernatant was discarded and the pellets were dried in hot air oven. As a result black color powder of Cs-FeNPs was obtained. Then the powder was transferred to a sterile amber bottle for further investigations.

Characterization of Cs-FeNPs:

Characterization of Cs-FeNPs was done by using UV-Vis spectrophotometer (Philips PU 8620), FT-IR (BRUKER, 600-3800 cm^{-1}, XRD (Malvern Panalytical) HR-TEM (JEOL JEM 1200 EXII) and SEM with EDX (Hitachi S 4160).

Antibacterial screening:

The antibacterial activity of Chitosan aqueous extract and Cs-FeNPs were screened against both Gram-positive (*Staphylococcus aureus* and *Enterococcus faecalis*) and Gram-negative bacteria (*Escherichia coli*, *Enterobacter*, *Klebsiella pneumonia*, *Pseudomonas aeruginosa*).

Well Diffusion Method:

The antibacterial activity of Chitosan aqueous extract and Cs-FeNPs were tested by standard well diffusion method (Boateng and Diunase, 2015). In the Bio safety chamber, 30 ml of Muller Hinton Agar (MHA) medium was poured into pre-sterilized Petri dishes and then the microorga-

Fig. 2: (A) Powdered form of Cs dissolved in DDW, (B) Cs aqueous extract (pale white colour), (C) Colour change of pale red colour was observed after adding Fe_3O_4 to the Cs aqueous extract, (D) Dark black colour synthesized Cs-FeNPs, (E) dark black colour Cs-FeNPs powder, and (F) Cs-FeNPs gets attracted towards the external magnetic field.

nisms was spreaded and suspended in the normal saline to create a confluent lawn bacterial growth with approximately 107 CFU (Colony Forming Unit). The media were then punched to form 6 mm diameter wells on the Muller- Hinton agar plates. Chitosan aqueous extract and Cs-FeNPs were poured into these wells of varying concentration of 10, 20, 30 and 40 µg/ml. Known antibiotics (Amikacin (30 µg/ml)) was used as positive standard labelled as AK. Finally, the Petri dishes were incubated for 24 h at 37°C. After incubation, plates were observed in the form of clear zone.

Results

The formation of Fe_3O_4 NPs were visually observed when colourless solution of chitosan aqueous extract showed a colour change from reddish to brownish-black precipitate (Fig. 2). The color shift from colorless to black happened due to the surface plasmon resonance (SPR) property of the material. Functional groups such as free amino and hydroxyl groups existing in CS might have joined with ferrous ions (FeII) and formed Fe-ellagate conjugate. Simultaneously, the formed conjugate leads to the nucleation that goes into reverse micellization, which later causes the reduction of Fe+ to nano-FeO.

UV Spectral analysis:

The UV-vis spectrophotometry analysis confirmed the formation of Cs-FeNPs. The broad peak at 233 nm indicates the synthesis of Fe_3O_4 NPs which gives rise to the surface plasmon resonance (SPR) adsorption band (Fig. 3). Hence, it was proven that Cs-FeNPs also can be synthesized using this one step reaction only. When the iron oxide is incorporated as composite, the absorbance band

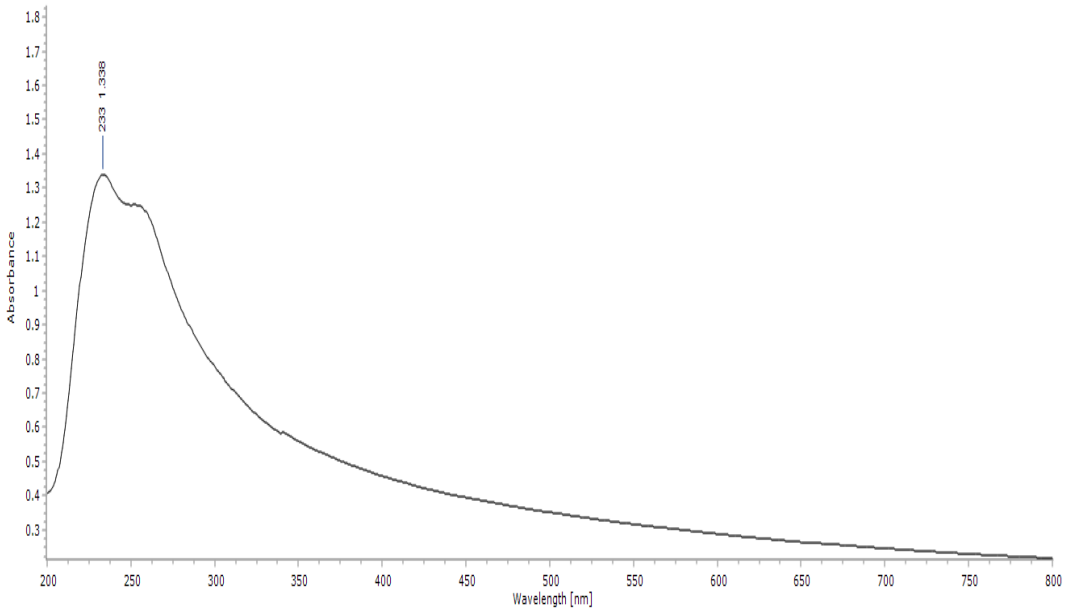

Fig. 3: UV spectral analysis of Cs-FeNPs.

at 220 nm has shifted to higher wavelength region with increased intensity. This absorption variation may be due to the association of iron oxide particles by successive loading within chitosan.

FT-IR spectral analysis:

To confirm the chemical composition of synthesized nanoparticles, FTIR spectra were obtained. It is used to understand the mechanism of formation of iron oxide and the related changes occurring in the particle size and particle size distribution of iron oxide. Figures 4 and 5 illustrate the FT-IR spectra of Cs aqueous extract and Cs-FeNPs. FTIR spectrum of chitosan aqueous extract gave the stretching vibrations at 3034cm^{-1} of OH stretch, 1504 cm^{-1} is assigned to C=O aromatic strong peaks bend scissoring, the peak at 1293 cm^{-1} to C-OH bend belongs to alkyl ketone, 1140 cm^{-1} to C–N stretch belongs to alkyl amines and C-H of secondary hydroxyl groups and 915.5 cm^{-1} to CH=CH alkalenes and aromatic in chitosan (Fig. 4). The spectra confirmed the conjugation of chitosan and Fe_3O_4 in the form of their functional group peaks. Thus these stretching vibrations at 915.5 cm^{-1}, 1140 cm^{-1}, 1293 cm^{-1}, 1504cm^{-1} and 3034 cm^{-1} with in the region of 600-3800 cm^{-1} represent the bonding of Cs aqueous extract and after bioreduction the peaks present in the Cs aqueous got disappeared. The FTIR spectrum of the synthesized Cs-FeNPs exhibited defined peaks at 649 cm^{-1}, 807 cm^{-1} and 1132 cm^{-1}. The vibrations at 649 cm^{-1} belongs to C-H stretch, 807 cm^{-1} of aromatic groups C-Br (strong) and C-F (strong) bond and 1132 cm^{-1} corresponds to the secondary hydroxyl groups denotes that these functional groups present in the Cs-FeNPs are responsible to act as a capping agent as shown in Figure 5. The appearance of well-defined peaks at 649 cm^{-1} was due to the vibrational intrinsic stretching of metal oxygen bond vibrations (here, it was Fe-O), which indicated that the developed NPs were iron oxide. Based on the result of FTIR, the functional groups of chitosan can be used as a reducing agent for the formation of Fe_3O_4 NPs and the chelation of iron with the presence of O–H and N–H of chitosan.

XRD spectral analysis:

X-ray diffraction analysis showed the presence of Fe_3O_4 particles with traces of Fe_2O_3 particles in the samples prepared. The crystalline of the Cs-FeNPs was examined by XRD as shown in Figure 6. The distinct peaks were found at 26, 33, 35, 55 and 62° accounting for crystal planes 012, 104, 113, 214

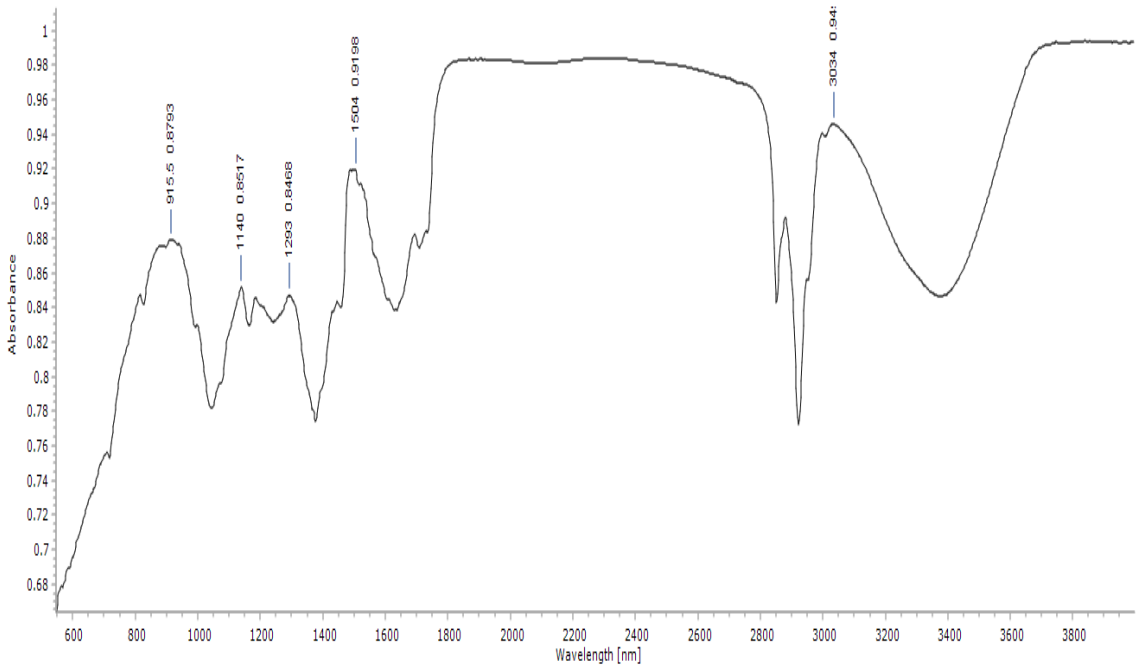

Fig. 4: FT-IR spectral image of Cs aqueous extract.

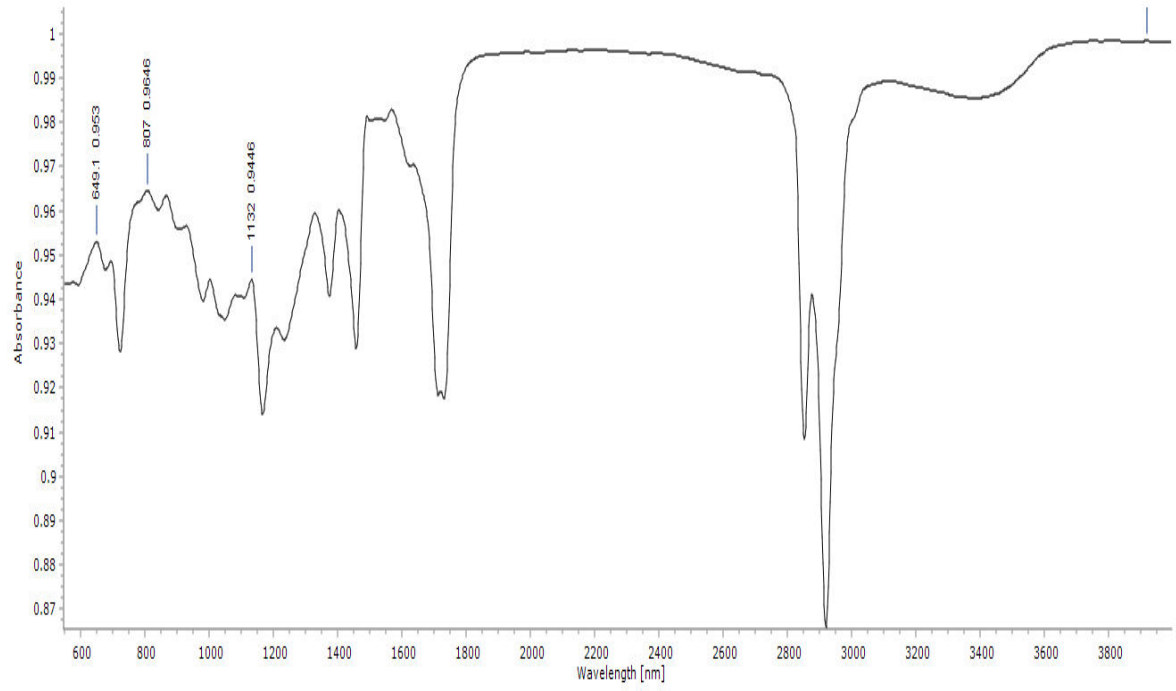

Fig. 5: FT-IR spectral image of Cs-FeNPs.

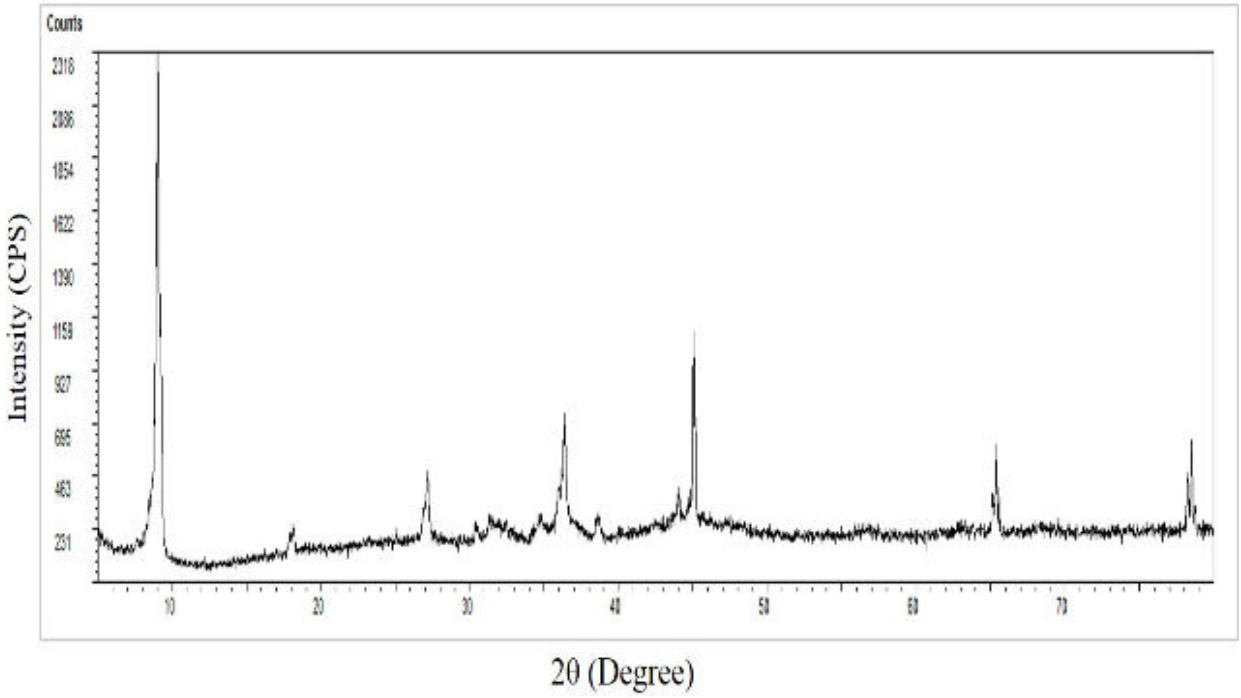

Fig. 6: XRD spectral image of Cs-FeNPs.

and 300, respectively. The graph was compared and found to be equal to the card JCPDS no. 34-0665 of hematite. The average crystal size was found out to be 28 nm in size by Scherrer equation. Based on the X-ray diffraction pattern, the synthesized Cs-FeNPs were figured out to be crystalline in nature.

HR-TEM Analysis:

The morphological characterization of the developed Cs-FeNPs was performed by transmission electron microscopy. The TEM image (Fig. 7) demonstrated the formation of spherical shaped Cs-FeNPs, which was found to be 3 to 5nm. Mostly, the NPs were well dispersed, whereas some of these were slightly agglomerated. The few large particles were found which could be due to the agglomeration of smaller particles; however, the majority of the particles in the TEM images were less than 100 nm in size. Moreover, Cs-FeNPs were affected with a magnetic field which can be observed in Figure 7.

SEM with EDX:

SEM image of the synthesized Cs-FeNPs showed that the particles were spherical in shape and highly agglomerated. Some distorted spherical shape particles was also seen in the image as shown in the Figure 8A-D. The EDX spectra were utilized for quantitative analysis of elements present in CsFeNPs. The EDAX spectrum showed the presence of light elements Fe in addition to O and C denotes contaminants which can be due to impurities from the substrate used during sample preparation (Fig. 9).

These light elements are present in high amount in Cs-FeNPs and its detection in the sample might have been from the Cs aqueous extract that was used during the synthesis process as shown in Figure 8. Thus the EDAX image confirmed that the iron oxide naoparticles was synthesized from the chitosan with the presence of Fe and O.

Antibacterial activity of chitosan aqueous extract and Cs-FeNPs:

The antibacterial activity of the Chitosan aqueous extract and Cs-FeNPs with different concentrations (10, 20, 30, 40 µg/ml) was evaluated against both Gram-positive (*E. faecalis*, *S. aureus*) and Gram-negative bacteria (*E. coli, Enterobacter, P. aeruginosa, K. pneumonia*) by disc diffusion technique. Amikacin was used in the experiment as a positive control. Experimental

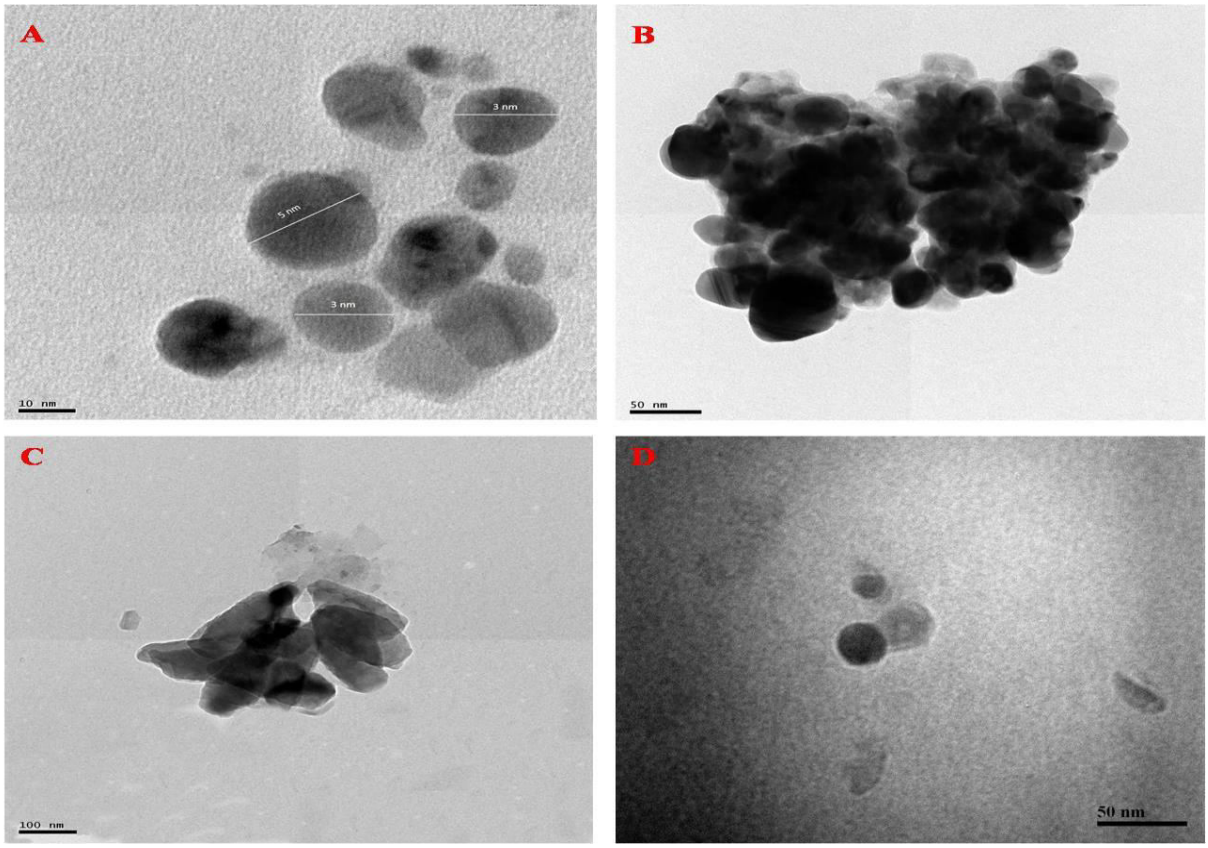

Fig. 7: HR-TEM image of the synthesized Cs-FeNPs at magnification of 10, 50 and 100 nm.

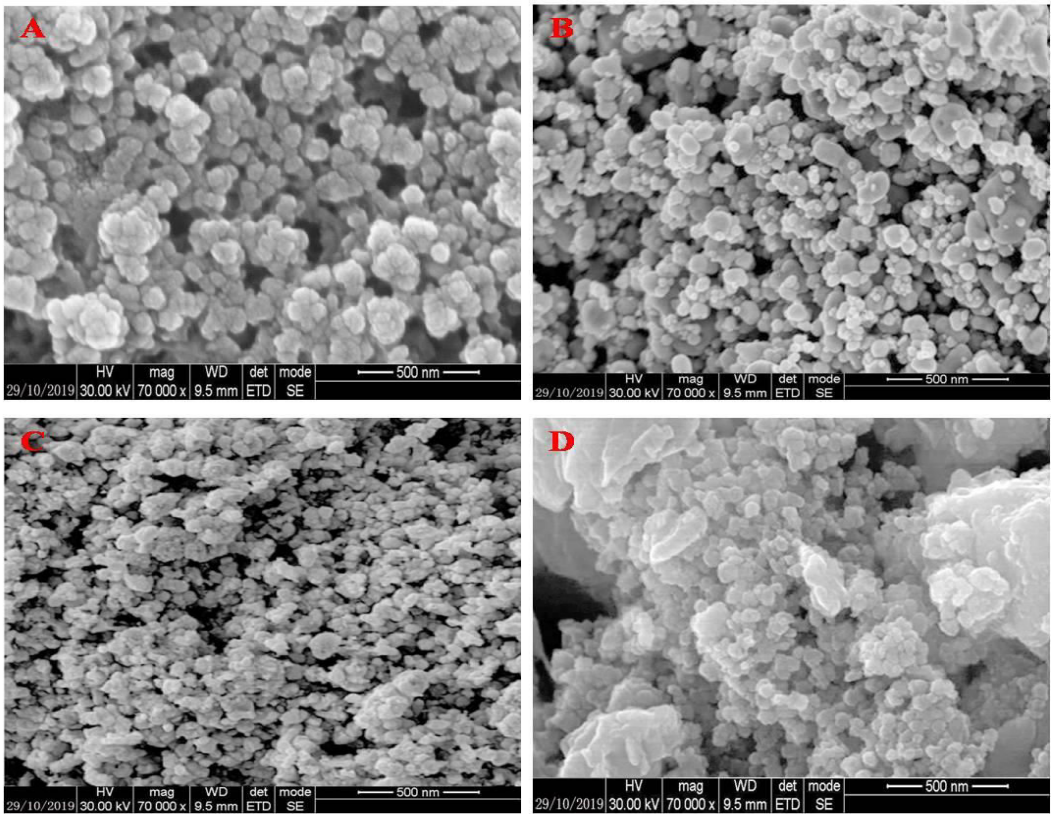

Fig. 8: SEM image of the synthesized Cs-FeNPs at magnification of 500 nm.

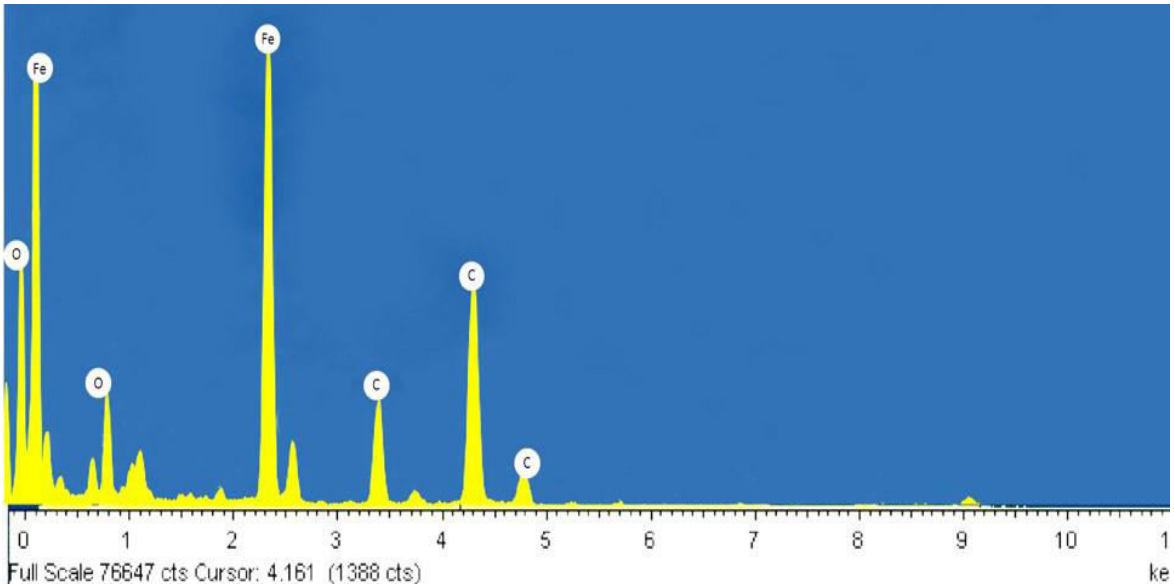

Fig. 9: EDAX spectrum of Cs-FeNPs.

Table 1: Zone of inhibition induced by Chiotsan aqueous extract

Name of the bacteria	**Zone of inhibition in mm**				
	AK	**10 µg/ml**	**20 µg/ml**	**30 µg/ml**	**40 µg/ml**
E. coli	15±0.57	5±0.33	6±0.57	7±0.33	8±0.57
K. pneumonia	17±0.33	7±0.58	9±0.33	9±0.58	15±0.58
P. aeruginosa	19±0.33	6±0.33	7±0.33	8±0.57	9±0.33
Enterobacter spp.	19±0.58	5±0.33	6±0.33	7±0.33	13±0.57
S. aureus	23±0.33	6±0.57	7±0.33	7±0.58	16±0.58
E. faecalis	15±0.57	5±0.33	6±0.57	7±0.57	8±0.57

Values are mean ± S.E. of six individual observations.

results were expressed as mean ± Standard error and deviations. The Chitosan aqueous extract showed minimum activity in all the tested bacterial species at 10 and 20 mg/ml. The activity increased only when concentration increased from 30 to 40 µg/ml (Table 1). Zone of inhibition formed was given in Figure 10 A. Highest zone of inhibition was observed in *S. aureus* (16±0.58 mm) at 40 µg/ml followed by *K. pneumoniae* (15± 0.58 mm), *Enterobacter* (13 ±0.57 mm), *P. aeruginosa* (9 ±0.33 mm), *E. faecalis* (8 ± 0.57 mm) and *E. coli* (8±0.57 mm) (Fig. 10B). Whereas, the positive control showed more activity than the aqueous extract which may be due to its antibiotic nature of the Amikacin. The antibacterial activity of Cs-FeNPs showed excellent antibacterial activity against all the tested species of bacteria which ranges from 17 to 22 mm. Cs-FeNPs was highly resistant to Amikacin and exhibited excellent zone of inhibition which is listed in Table 2. The zone of inhibition formed was given in Figure 11A. The Cs-FeNPs showed an excellent antibacterial activity against *K. Pneumoniae* and the zone of inhibition was found to be *(*22±0.58 mm) at 40 µg/ml (Fig. 11B). In general Cs-FeNPs was more effective against both the bacterial

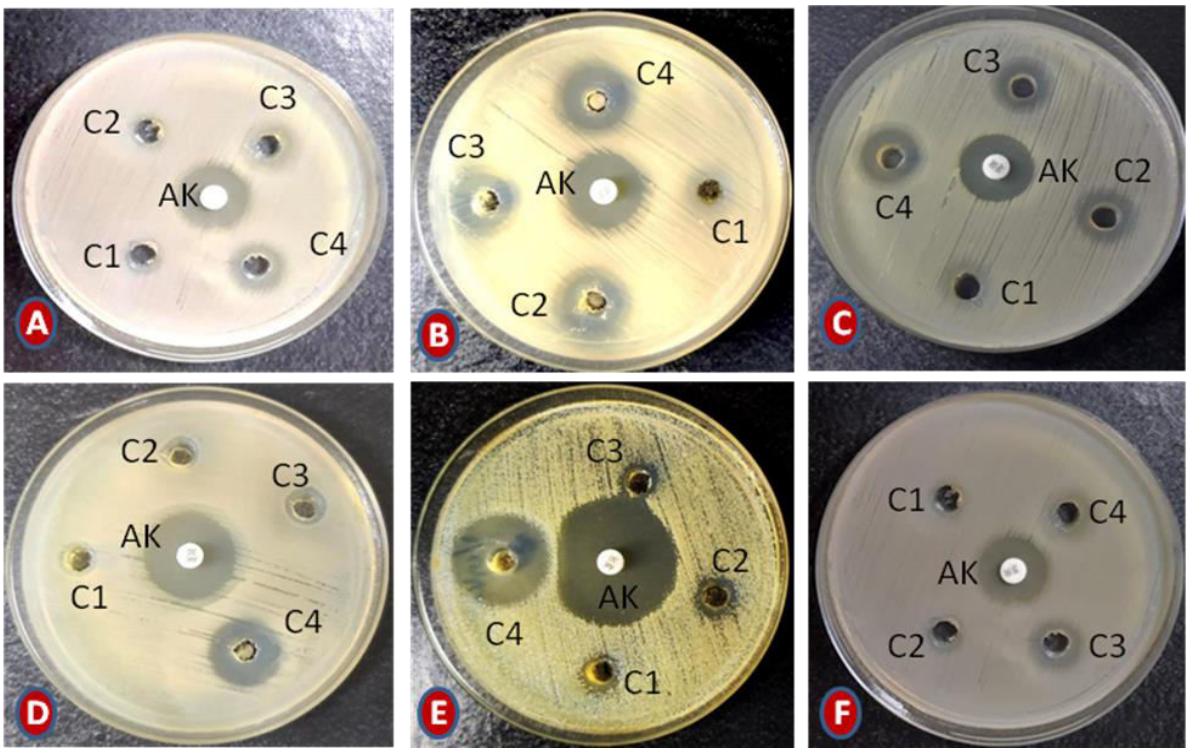

Fig. 10 A: Photograph showing the discs of antibacterial activity of chitosan aqueous extract against various ATCC strains. (A) *E. coli*, (B) *K. pneumoniae*, (C) *P. aeruginosa*, (D) *Enterobacter*, (E) *S. aureus* and (F) *E. faecalis.* Key: C1, C2, C3 and C4 denotes 10 µg/ml, 20 µg/ml, 30 µg/ml and 40 µg/ml; AK= Amikacin 30 µg/ml.

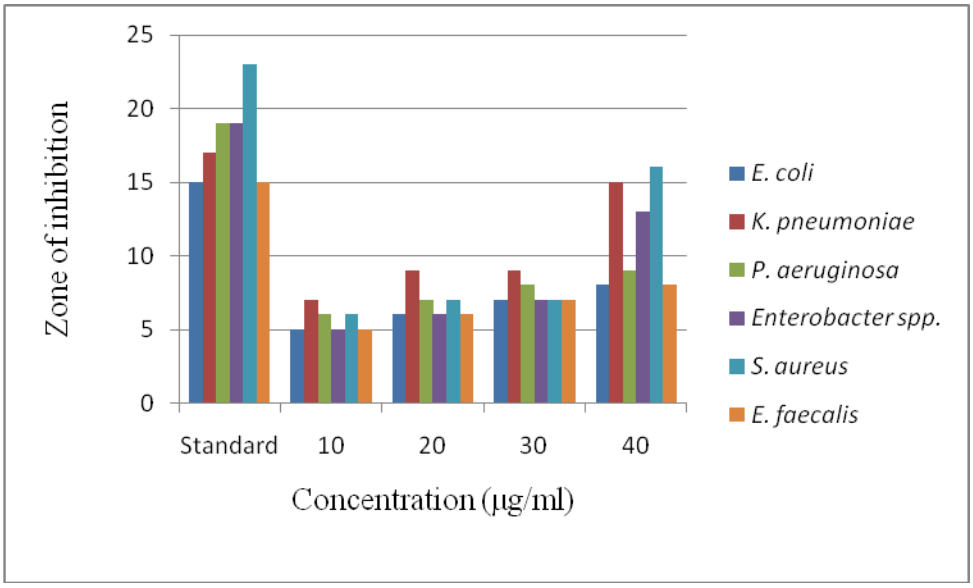

Fig. 10 B: Antibacterial activity of chitosan aqueous extract against various ATCC strains.

Table 2: Zone of inhibition induced by Cs-FeNPs

Name of the bacteria	Zone of inhibition in mm				
	AK	10 µg/ml	20 µg/ml	30 µg/ml	40 µg/ml
E. coli	15±0.33	9±0.58	12±0.33	15±0.58	19±0.57
K. pneumoniae	17±0.57	8±0.57	11±0.58	17±0.33	22±0.58
P. aeruginosa	22±0.33	9±0.58	10±0.57	13±0.57	18±0.33
Enterobacter spp.	16±0.57	8±0.33	11±0.58	14±0.57	18±0.33
S. aureus	19±0.58	9±0.33	11±0.33	15±0.58	19±0.33
E. faecalis	10±0.33	8±0.57	11±0.33	14±0.57	17±0.33

Values are mean ± S.E. of six individual observations.

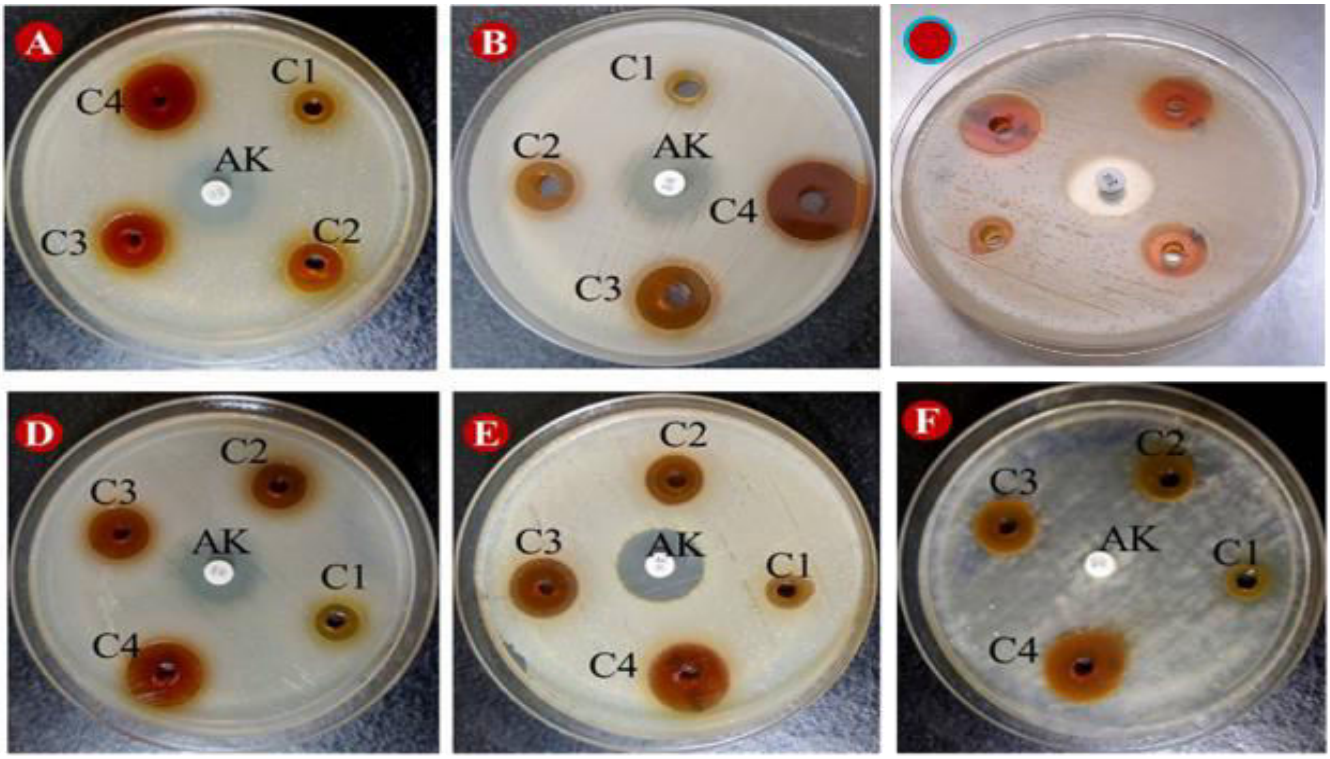

Fig. 11 A: Photograph showing the discs of antibacterial activity of synthesized Cs-FeNPs against various ATCC strains. (A) *E. coli*, (B) *K. pneumoniae*, (C) *P. aeruginosa*, (D) *Enterobacter* , (E) *S. aureus* and (F) *E. faecalis.*
Key: C1, C2, C3 and C4 denotes 10 µg/ml, 20 µg/ml, 30 µg/ml and 40 µg/ml; AK=Amikacin 30 µg/ml

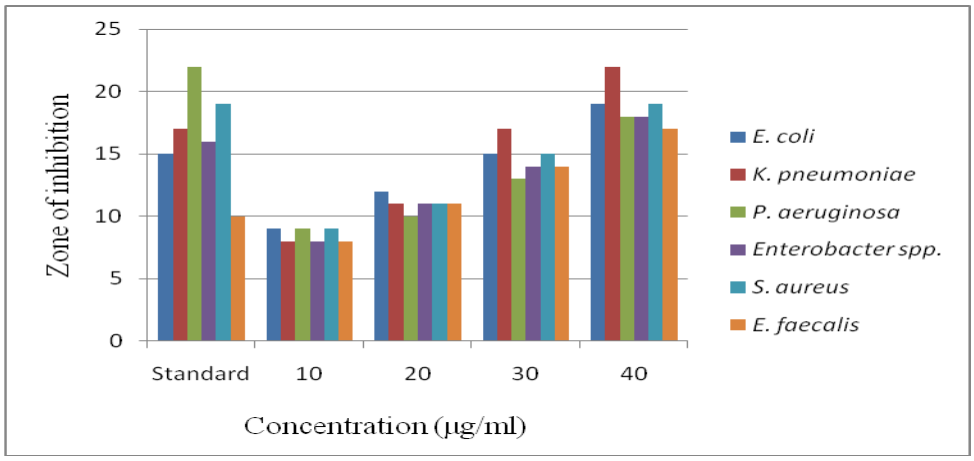

Fig. 11 B: Antibacterial activity of synthesized Cs-FeNPs against various ATCC strains.

strains than the aqueous extract of chitosan.

Discussion

Recently, iron oxide and ferrites such as maghemite (γ-Fe_2O_3) have attracted the attention of researchers because of their unique size, physical properties, and their wide applications in different processes as a result of their controllable sizes, shapes and compositions (Janardhanan *et al.,* 2008). Furthermore, coating metal oxide magnetic nanoparticles with chemically active polymers such as chitosan can protect them from oxidation and provide amino functional groups for attachment (Sahin *et al.,* 2016; Naskar *et al.,* 2018).

Chitosan (Cs) is a natural biopolymer with comprehensive biological and chemical properties which makes it suitable for use in pharmaceutical, commercial and biomedical applications (Vaseashta *et al.,* 2008; Kravanja *et al.,* 2019) which has been used to coat the surface of Iron oxide nanoparticles (Chen *et al.,* 2012; Podrepšek *et al.,* 2020). Structurally Cs consists of amino and hydroxyl functional groups that enable Cs to easily graft to the surface of iron oxide nanoparticles. Thereby Cs enhances the stability, biocompatibility and biodegradability of Iron oxide nanoparticles (Kim *et al.,* 2008; Akakuru *et al.,* 2018). Results revealed that Chitosan is potential biomolecules that can be employed for Cs-FeNPs synthesis since it is non-toxic, hydrophilic, biocompatible and biodegradable (Safdar *et al.,* 2018; Sonin *et al.,* 2020).

UV–vis analysis is useful in the characterization of NPs and provides certain information regarding the stability, shape, and size of the NPs (Deshmukh *et al.,* 2019). Kavitha (2017) stated that the synthesis of the iron oxide using chitosan from crab shells gives absorption band at 226 nm may be due to the absorption and scattering of light by iron oxide particles and its characteristics of the indirect band gap of semiconductors. When the iron oxide is incorporated as composite, the absorbance band at 220 nm has shifted to higher wavelength region with increased intensity. This absorption variation may be due to the association of iron oxide particles by successive loading within chitosan. Samrot *et al.* (2018) also identifed SPR peaks at 225 and 360 nm in the uncoated and chitosan-coated iron oxide nanoparticles, respectively. Appu *et al.* (2021) reported that the UV spectral analysis of chitosan (Cs)-coated iron oxide (Fe_3O_4) nanocomposites (NCs) by employing the aqueous leaf extract of *Brassica oleracea* L. showed peak at 290 nm due to strong surface plasmon resonance (SPR). Similarly, Boudouh *et al.* (2021) documented the exhibition of black color during the fabrication of FeO NPs. The Cs-FeNPs has displayed a maximum absorbance peak at 233 nm and thus indicated a convenient surface plasmon resonance character for FeO nanoparticles. The findings of present study are in agreement with observations of Bibi *et al.* (2019) and Abdullah *et al.* (2020).

The FTIR analysis results were consistent with the confirmation accomplished from other additional executed characterization results. Narrower absorption peaks at 649 cm^{-1} of Cs-FeNPs are supposed owing to the presence of metal–oxygen (Fe–O), which matched with several studies (Amutha and Sridhar 2018; Abdullah *et al.,* 2020; Aziz *et al.,* 2020; Appu *et al.,* 2021). The characteristic shoulder peaks of chitosan at 1504 cm^{-1} corresponding to the stretching peaks of the amide C=O bonds shifted to 1132 cm^{-1} which is due to the covalent bond that is established between the amino groups of chitosan molecules and propyl-(1H-tetrazole-5-yl) amine-trimethoxysilane and some of the peaks were disappeared due to bioreduction of the functional groups proved the formation of Cs-FeNPs (Kashkouli *et al.,* 2018; Siddeeg *et al.,* 2020). Besides, $-NH_3$ groups of chitosan are attracted by –OH- of iron oxide, through this way nuclear growth of iron oxide is inhibited by chitosan molecules which provides smaller core size. In comparison with the chitosan spectrum, all the significant peaks of chitosan in the range of 600-3800 cm^{-1} are present in the Cs-FeNPs with a small shift. Additionally, the C–O absorption peak of

secondary hydroxyl group becomes stronger and moves from chitosan 1140 cm^{-1} to 1132 cm^{-1}in Cs-FeNPs. Finally, the absorption of Fe–O bond of Fe_3O_4 still exists in the Cs-MNPs, which further demonstrates that Fe_3O_4 nanoparticles have been wrapped by cross linked chitosan, and the results are in good agreement with the conclusions of XRD analyses.

Transmission electron microscopy (TEM) is a widely used tool for studying organelle ultrastructure. TEM produces high-resolution images by transmitting electrons through an ultrathin section of the sample and magnifying the resulting image using a series of lenses (Facility, 2021). TEM has enabled researchers to study the ultrastructure of organelles in a wide variety of healthy and diseased cells and tissues, yielding important insights into cellular processes and disease development (Franken *et al.,* 2020). During a study conducted by Zeinali *et al.* (2016), chitosan capped SPIONS averaged at 13.5, 9.6 and 7.7 nm were accomplished, during the work sonication times were varied with an increase in the sonication time resulting in smaller sized particles. This was reasoned by the fact that prolonged sonication times resulted in higher degree of agglomeration. Similarly, earlier studies have reported that aqueous solution and neutral pH can increase the aggregation in FeO NPs (Herlekar *et al.,* 2014; Kannan *et al.,* 2019; Sathiyaseelan *et al.,* 2021). Synthesis of Iron-Oxide Nanoparticles (FeNPs) and Bacterial Cellulose Impregnated with Iron-Oxide Nanoparticles was carried out by Patwa *et al.* (2020). The nanoparticles had a spherical morphology with average particle size of 47.2 ± 13.7 nm. As can be seen from the micrograph, the nanoparticles tended to form agglomerates consisting of 2–3 particles which increased the overall particle size.

XRD analysis resulted that the distinct peaks were found at 26, 33, 35, 55 and 62° accounting for crystal planes 012, 104, 113, 214 and 300, respectively. These characteristic peaks are in agreement with standard diffraction data JCPDS: 34-0665 of hematite and correspond to face-centered cubic (fcc) symmetry (Asuha *et al.,* 2009; Samuel *et al.,* 2021). In addition, earlier reports found that Fe_3O_4 nanoparticle crystallinity was not changed by the chitosan coating (Li *et al.,* 2008). Badry *et al.* (2022) showed results on XRD patterns of chitosan nanocomposites which exhibited a typical α-Fe_2O_3 structure where eleven characteristic peaks are observed for α-Fe_2O_3 nanoparticles (2θ = 24.1°, 33.1°, 35.6°, 40.7°, 49.4°, 54.0°, 57.4°, 62.3°, 63.9°, 71.8° and 75.3°) marked by their indices [(012), (104), (110), (113), (024), (116), (018), (214), (300), (1010) and (220), respectively]. Villamin and Yoshitaka (2021) stated the XRD results of the samples with different chitosan concentrations have XRD peaks corresponding mostly to the Fe_3O_4 standard peaks. The obtained diffraction peaks are having lattice parameter a = 8.39 Å and results are in good agreement with the standard data (JCPDS: 19-0629) (Chaki *et al.,* 2015; Agnes *et al.,* 2022).

SEM is the leading tool that is capable of achieving a detailed visual image of a particle with high-quality and spatial resolution of 1 nm (Brabazon and Raffer, 2010; Akhtar *et al.,* 2018). Pérez-Beltrán *et al.* (2021) demonstrated that The SEM investigation of FeONPs displayed a spherical shaped particle. Hebzi and Helen (2020) stated that iron oxide nanoparticles synthesized from crustacean waste crab shells showed the scanning electrons microscopic image which showed the high density of iron oxide nanoparticles synthesized by chitosan. Thus, the EDAX image confirms that the iron oxide naoparticles was synthesized from the chitosan with the presence of Fe and O. The present results are in conformity with reports of Braim *et al.* (2022).

According to our study, the synthesis of Cs-FeNPs through an eco-friendly method. Natural polymers such as Cs have been employed as templates at which Fe (II) centers initially interact to form complexes. The complexes were subsequently treated under controlled conditions to generate Cs-FeNPs (Aurich *et al.,* 2007; Sun *et al.,* 2017; Deng *et al.,* 2019; Ajinkya *et al*., 2020) where the polysaccharide template provided for

capping or encapsulation to separate the synthesized NP, this feature uses templates to provide binding sites for Fe (II) centers, which are then spatially separated and can therefore be synthesized efficiently and size reduction through controlled removal of templates.

However, this study suggested that the Cs-FeNPs showed better activity against Gram positive bacteria when compared to Gram-negative strains. This has happened because the Gram-negative bacteria usually own an extra outer layer of lipopolysaccharide and peptidoglycan which helps the gram-negative bacteria reduce the damage that might be caused by Cs-FeNPs. Regardless of the mechanism, which has yet to be established, these findings demonstrated the crucial role of the capping agent for antibacterial properties. Therefore, the capping agent also contributes to or negates the toxicity of this material. We can speculate that a complete Chitosan cap may also reduce the toxicity of NPs known to exhibit cytotoxic effects in both *in vivo* as well as *in vitro* studies. Even at high concentrations, we might expect to observe some inhibition due to incomplete coverage in the Chitosan aqueous extract, however, that is not the case.

In the case of Cs-FeNPs the bacterial inhibition was higher when the concentration was increased. The findings concluded that Cs-FeNPs has antibacterial activity at relatively very high concentrations due to its strong binding affinity of its functional group. This causes changes in the interaction pattern at the Nano-bio interface; hence play crucial role in determining the antibacterial propensity of Cs-FeNPs. However, the enhanced production of reactive oxygen species because of the interaction potential at the interface is the principal cause for the antimicrobial propensity of the NPs. As a conclusion, the interaction pattern at the Nano-bio interface plays vital role in determining the antibacterial activity of Cs-FeNPs.

Due to the low solubility of FeNPs in water, they tend to agglomerate, have short residence time in the host, and the needs to use toxic solvents during synthesis, their clinical application were restricted. As a solution to these challenges, some studies have employed chitosan as a coating on the FeNPs. For example, Yanwu Zhai *et al*. (2022) synthesized chitosan-coated iron oxide nanoparticles (Cs-FeNPs) using chitosan with various molecular weights, and optimized their function by varying the concentration of chitosan in the solution. From their research, they successfully synthesized mono-dispersed NPs sized from 2 nm to 5 nm. The suspension of Cs-FeNPs was clear and transparent, indicating they had excellent water dispersion (Bharathi *et al.,* 2019). The only problem of Cs-FeNPs was that they tended to agglomerate at a higher pH. However, this could be solved by adding more chitosan to the Cs-FeNPs suspension. Senthilkumar and Venkatesalu (2013) synthesized Cs-FeNPs and tested their antimicrobial property against both Gram-positive (*S. aureus* and *E. faecalis*) and Gram-negative bacteria (*E. coli*, *Enterobacter, K. pneumoniae*, *P. aeruginosa*) (Senthilkumar and Venkatesalu, 2013; Kalaivani *et al.,* 2018). They found that, due to the direct interaction with the cell membrane of bacteria, Cs-FeNPs greatly influenced the morphology of Gram-positive (*S. aureus* and *E. faecalis*) and Gram-negative bacteria (*E. coli*, *Enterobacter, K. pneumoniae, P. aeruginosa)*, helping to kill the bacteria (Maria Dhivya *et al*., 2016; Mirza *et al.,* 2018; Gingasu *et al.,* 2018).

Conclusion

In recent years, attentions are focused on metal NPs, especially Cs-FeNPs. These NPs has potential antimicrobial uses in addition to other environmental uses. However, large-scale production of these NPs is still limited. The synthesis of NPs is an important requirement for identifying individual biomaterials required for commercial applications in accordance with commercial parameters and obtaining the required amount of NPs in individual quantities. So far, a large number of reports have been published in the eco- friendly production of silver

and gold NPs; however, only Cs-FeNPs were synthesized and evaluated for various applications at the research level. Commercial use of these NPs is especially important for the treatment of cancer for biomedical use as regular chemotherapy methods have many side effects on patients. A NPs-coated drug injected using a magnetic field can target normal, healthy cells at the point of death without injury, leading to a specific approach to pointing to the cancer cell destruction site.

References

Abdallah Y, Liu M, Ogunyemi SO, Ahmed T, Fouad H, Abdelazez A, Yan C, Yang Y, Chen J and Li B. (2020) Bioinspired green synthesis of chitosan and zinc oxide nanoparticles with strong antibacterial activity against rice pathogen *Xanthomonas oryzae* pv. *oryzae*. Molecules 25(20): 4795.

Abdullah JAA, Eddine LS, Abderrhmane B, Alonso-González M, Guerrero A and Romero A. (2020) Green synthesis and characterization of iron oxide nanoparticles by *Pheonix dactylifera* leaf extract and evaluation of their antioxidant activity. Sustain Chem Pharm. 17: 100280.

Agnes J, Ajith P, Sappani Muthu M and Premanand D (2022) Synthesis and characterization studies of mesostructured chitosan coated Fe_3O_4 nanoparticles with folic acid. Int J Engineer Adv Technol. 11(4): 135-141.

Ajinkya N, Yu X, Kaithal P, Luo H, Somani P and Ramakrishna S. (2020) Magnetic iron oxide nanoparticle (IONP) synthesis to applications: Present and future. Materials 13(20): 4644.

Akakuru OU, Louis H, Amos PI, Akakuru OC, Nosike EI and Ogulewe EF. (2018) The chemistry of chitin and chitosan justifying their nanomedical utilities. Biochem Pharmacol. 7: 1000241.

Akhtar K, Khan SA, Khan SB and Asiri AM. (2018) Scanning electron microscopy: Principle and applications in nanomaterials characterization. In: Handbook of materials characterization, (ed.) Sharma S.K., Springer International Publishing, pp. 113-145.

Appu M, Lian Z, Zhao D and Huang J. (2021) Biosynthesis of chitosan-coated iron oxide (Fe_3O_4) hybrid nanocomposites from leaf extracts of *Brassica oleracea* L. and study on their antibacterial potentials. 3 Biotech. 11(6): 271.

Arias LS, Pessan JP, Vieira APM, Lima TMTD, Delbem ACB and Monteiro DR. (2018) Iron oxide nanoparticles for biomedical applications: a perspective on synthesis, drugs, antimicrobial activity, and toxicity. Antibiotics 7(2): 46.

Asuha S, Zhao S, Wu H, Song L and Tegus O. (2009) One step synthesis of maghemite nanoparticles by direct thermal decomposition of Fe–urea complex and their properties. J Alloys Compd. 472: L23-L25.

Aurich K, Schwalbe M, Clement JH, Weitschies W and Buske N. (2007) Polyaspartate coated magnetite nanoparticles for biomedical applications. J Magnetism Magnetic Materials 311(1): 1-5.

Aziz A, Nisar A, Khan A, Muhammad B, Malik S, Nauman A and Hamayun K. (2020) Chitosan-zinc sulfide nanoparticles, characterization and their photocatalytic degradation efficiency for azo dyes. Int J Biol Macromolec. 153: 502-512.

Azizi A. (2020) Green synthesis of Fe_3O_4 nanoparticles and its application in preparation of Fe_3O_4/cellulose magnetic nanocomposite: A suitable proposal for drug delivery systems. J Inorg Organometallic Polymers Materials 30: 3552-3561.

Badry MD, Mohammed AW, Rabab KK and Mamdouh MA. (2022) Hydrothermally assisted synthesis of magnetic iron oxide-chitosan nanocomposites: Electrical and biological evaluation. Biointerface Res Appl Chem. 12(2): 2229-2241.

Bharathi D, Ranjithkumar R, Vasantharaj S, Chandarshekar B and Bhuvaneshwari V. (2019) Synthesis and characterization of chitosan/iron oxide nanocomposite for biomedical applications. Int J Biol Macromolec. 132: 880–887.

Bibi I, Nazar N, Ata, S, Sultan M, Ali A, Abbas A, Jilani K, Kamal S, Sarim FM and Khan MI. (2019) Green synthesis of iron oxide nanoparticles using pomegranate seeds extract and photocatalytic activity evaluation for the degradation of textile dye. J Mater Res Technol. 8: 6115-6124.

Boudouh D, Hamana D, Metselaar HSC, Achour S, Chetibi, L and Akhiani AR. (2021) Low-temperature green route synthesis of Fe3O4 -C nanocomposite using olive leaves extract. Mater Sci Eng B 271: 115276.

Brabazon D and Raffer A. (2010) Advanced characterization techniques for nanostructures. In: Emerging nanotechnologies for manufacturing, (eds.) Ahmed W. and Jackson M.J., Boston: William Andrew Publishing, pp. 59-91.

Braim FS, Nik Noor Ashikin Nik Ab Razak, Azlan Abdul A, Layla Qasim I and Bashiru Kayode S. (2022) Ultrasound assisted chitosan coated iron oxide nanoparticles: Influence of ultrasonic irradiation on the crystallinity, stability, toxicity and magnetization of the functionalized nanoparticles. Ultrasonics Sonochem. 88: 106072.

Chaki SH, Tasmira J, Malek MD, Chaudhary JP, Tailor and Deshpande MP. (2015) Magnetite Fe_3O_4 nanoparticles synthesis by wet chemical reduction and their characterization. Adv Nat Sci Nanosci Nanotechnol. 6(3): 035009.

Chen HJ, Zhang ZH, Luo LJ and Yao SZ. (2012) Surface-imprinted chitosan-coated magnetic nanoparticles modified multi-walled carbon nanotubes biosensor for detection of bovine serum albumin. Sensors Actuators B Chem. 163: 76-83.

Deng ZY, Chen KL and Wu CH. (2019) Improving the SERS signals of biomolecules using a stacked biochip containing Fe_2O_3/Au nanoparticles and a DC magnetic field. Scient Rep. 9(1): 1-8.

Deshmukh AR, Gupta A and Beom Soo K. (2019) Ultrasound assisted green synthesis of silver and iron oxide nanoparticles using fenugreek seed extract and their enhanced antibacterial and antioxidant activities. BioMed Res Int. 2019: 1714358.

Facility, The University of Iowa's Central Microscopy Research Facility Methodology. https://cmrf. research. uiowa.edu/

Filser J, Arndt D, Baumann J, Geppert M, Hackmann S, Luther EM, Christian P, Prenzel K, Wigger H, Jürgen A, Michaela CH, Köser J, Kück A, Lesnikov E, Jennifer Neumann, Simon Schütrumpf, Jürgen Warrelmann, Marcus Bäumer, Ralf Dringen, Arnim von Gleich, Petra Swiderek and Thöming J. (2013) Intrinsically green iron oxide nanoparticles? From synthesis via (eco-) toxicology to scenario modelling. Nanoscale 5(3): 1034-1046.

Franken LE, Grünewald K, Boekema EJ and Stuart MCA. (2020) A technical introduction to transmission electron microscopy for soft-matter: Imaging, possibilities, choices, and technical developments. Nano Micro Small 16(14): 1906198.

Gaiani G, O'Sullivan CK and Campàs M. (2019) Magnetic beads in marine toxin detection: A review. Magnetochem. 5(4): 62.

Gingasu D, Mindru I, Patron L, Ianculescu A, Vasile E, Marinescu G, Preda S, Diamandescu L, Oprea O, Popa M, Saviuc C and Chifiriuc MC. (2018) Synthesis and characterization of chitosan-coated cobalt ferrite nanoparticles and their antimicrobial activity. J Inorg Organomet Polym Mater. 28: 1932-1941.

Guo B, Li M and Li S. (2020) The comparative study of a homogeneous and a heterogeneous system with green synthesized iron nanoparticles for removal of Cr (VI). Scient Rep. 10(1): 1-11.

Hebzi ERM and Helen MS. (2021) Synthesis of chitosan encapsulated iron oxide nanoparticles and its biomedical application. Int J Aquat Sci. 12(2): 4981-4985.

Herlekar M, Barve S and Kumar R. (2014) Plant-mediated green synthesis of iron nanoparticles. J Nanopart. 2014: 140614.

Hernández-Hernández AA, Aguirre-Álvarez G, Cariño-Cortés R, Mendoza-Huizar LH and Jiménez-Alvarado R. (2020) Iron oxide nanoparticles: synthesis, functionalization, and applications in diagnosis and treatment of cancer. Chemical Papers 74: 3809-3824.

Janardhanan SK, Ramasamy I and Nair BU. (2008) Synthesis of iron oxide nanoparticles using chitosan and starch templates. Transit Met Chem. 33: 127-131.

Kalaivani R, Maruthupandy M, Muneeswaran T, Hameedha Beevi A, Anand M, Ramakritinan CM and Kumaraguru AK. (2018) Synthesis of chitosan mediated silver nanoparticles (Ag NPs) for potential antimicrobial applications. Front Lab Med. 2(1): 30-35.

Kannan D, Yadav N, Ahmad S, Namdev P, Bhattacharjee S, Lochab B and Singh S. (2019) Pre-clinical study of iron oxide nanoparticles fortified artesunate for efficient targeting of malarial parasite. EBioMed. 45: 261-277.

Kashkouli KI, Mahani MT and Mosaddegh E. (2018) Synthesis and characterization of aminotetrazole-functionalized magnetic chitosan nanocomposite as a novel nanocarrier for targeted gene delivery. Mater Sci Eng C 89: 166-174.

Katz, E. (2020). Magnetic nanoparticles. Magnetochem. 6(1): 6.

Kavitha AL. (2017) Synthesis and characterization of iron oxide-chitosan nano composite. Mechanics Mater Sci Engineer. 13. doi: 10.2412/mmse.92. 76.971.

Khan R, Rehman A, Hayat A and Andreescu S. (2019) Magnetic particles-based analytical platforms for food safety monitoring. Magnetochem. 5(4): 63.

Kim M, Lee JH and Nam JM. (2019) Plasmonic photothermal nanoparticles for biomedical applications. Adv Sci. 6(17): 1900471.

Kim Y, Seo SJ, Moon HS, Yoo MK, Park IY, Kim BC and Cho CS. (2008) Chitosan and its derivatives for tissue engineering applications Biotechnol Adv. 26: 1-21.

Kravanja G, Primožiˇc M, Knez Ž and Leitgeb M. (2019) Chitosan-based (Nano) materials for novel biomedical applications. Molecules 24: 1960.

Li G, Jiang Y, Huang K, Ding P and Chen J. (2008) Preparation and properties of magnetic Fe_3O_4–chitosan nanoparticles. J Alloy Compd. 466: 451-456.

Maria DS, Sathiya SM, Manivannan G and Jothi Rajan MA. (2016) A comparative study on the biopolymer functionalized iron oxide nanocomposite for antimicrobial activity. Mater Today Proc 3(10): 3866-3871.

Mirza AU, Kareem A, Nami SAA, Shoeb Khan M, Rehman S, Bhat SA, Mohammad A and Nishat N. (2018) Biogenic synthesis of iron oxide nanoparticles using *Agrewia optiva* and *Prunus persica* phyto species: Characterization, antibacterial and antioxidant activity. J Photochem Photobiol B Biol. 185: 262-274.

Moise S, Céspedes E, Soukup D, Byrne JM, El Haj AJ and Telling ND. (2017) The cellular magnetic response and biocompatibility of biogenic zinc-and cobalt-doped magnetite nanoparticles. Scient Rep. 7(1): 1-11.

Nadeem Baig, Irshad K and Wail F. (2021) Nanomaterials: a review of synthesis methods, properties, recent progress, and challenges. Mater Adv. 2: 1821-1871.

Nadia G Kandile, Howida T Zaky, Mansoura I Mohamed, Abir S Nasr and Yassmin GA. (2018) Extraction and characterization of chitosan from shrimp shells. Open J Organic Polymer Mater. 8: 33-42.

Naskar S, Sharma S and Kuotsu K. (2018) Chitosan-based nanoparticles: An overview of biomedical applications and its preparation. J Drug Deliv Sci Technol. 49: 66-81.

Patel S, Jana S, Chetty R, Thakore S, Singh M and Devkar R. (2019) Toxicity evaluation of magnetic iron oxide nanoparticles reveals neuronal loss in chicken embryo. Drug Chemical Toxicol. 42(1): 1-8.

Patwa R, Zandraa O, Capáková Z, Saha N and Sáha P. (2020) Effect of iron-oxide nanoparticles impregnated bacterial cellulose on overall properties of alginate/casein hydrogels: Potential injectable biomaterial for wound healing applications. Polymers 12(11): 2690.

Pérez-Beltrán CH, García-Guzmán JJ, Ferreira B, Estévez-Hernández O, López-Iglesias D, Cubillana-Aguilera L, Link W, Stănică N, Rosa da Costa AM and Palacios-Santander JM. (2021) One-minute and green synthesis of magnetic iron oxide nanoparticles assisted by design of experiments and high energy ultrasound: Application to biosensing and immunoprecipitation. Mater Sci Eng C Mater Biol Appl. 123: 112023.

Plachtová P, Medrikova Z, Zboril R, Tucek J, Varma RS and Maršálek B. (2018) Iron and iron oxide nanoparticles synthesized with green tea extract: differences in ecotoxicological profile and ability to degrade malachite green. ACS Sustainable Chem Engineer. 6(7): 8679-8687.

Podrepšek GH, Knez Z and Leitge M. (2020) Development of chitosan functionalized magnetic nanoparticles with bioactive compounds. Nanomaterials 10: 1913.

Safdar R, Omar AA, Arunagiri A, Iyyaswami R and Thanabalan M. (2018) Potential of chitosan and its derivatives for controlled drug release applications--A review. J Drug Deliv Sci Technol. 49: 642-659.

Sahin S and Ozmen I. (2016) Determination of optimum conditions for glucose-6-phosphate dehydrogenase immobilization on chitosan-coated magnetic nanoparticles and its characterization. J Mol Catal B Enzym. 133: S25-S33.

Saif S, Tahir A and Chen Y. (2016) Green synthesis of iron nanoparticles and their environmental applications and implications. Nanomaterials 6(11): 209.

Salimi M, Sarkar S, Fathi S, Alizadeh AM, Saber R, Moradi F and Delavari H. (2018) Biodistribution, pharmacokinetics, and toxicity of dendrimer-coated iron oxide nanoparticles in BALB/c mice. Int J Nanomed. 13: 1483.

Samrot AV, Ujjala B, Sheryl AP, Shobana N and Kumar C. (2018) Synthesis of curcumin loaded polymeric nanoparticles from crab shell derived chitosan for drug delivery. Informatics Med Unlocked 10: 159-182.

Samuel MS, Datta S, Chandrasekar N, Balaji R, Selvarajan E and Vuppala S. (2021) Biogenic synthesis of iron oxide nanoparticles using *Enterococcus faecalis*: Adsorption of hexavalent chromium from aqueous solution and in vitro cytotoxicity analysis. Nanomaterials 11: 3290.

Sathiyaseelan A, Saravanakumar K, Mariadoss AVA and Wang MH. (2021) Antimicrobial and wound healing properties of FeO fabricated chitosan/PVA nanocomposite sponge. Antibiotics 10(5): 524.

Senthilkumar A and Venkatesalu V. (2013) Chemical constituents, *in vitro* antioxidant and antimicrobial activities of essential oil from the fruit pulp of wood apple. Indust Crops Prod. 46: 66-72.

Shevtsov M, Nikolaev B, Marchenko Y, Yakovleva L, Skvortsov N, Mazur A, Tolstoy P, Ryzhov V and Multhoff G. (2018) Targeting experimental orthotopic glioblastoma with chitosan-based superparamagnetic iron oxide nanoparticles (CS-DX-SPIONs). Int J Nanomed. 13: 1471-1482.

Siddeeg SM, Mohamed AT, Wissem M and Faouzi Ben R. (2020). Iron oxide/chitosan magnetic nanocomposite immobilized manganese peroxidase for decolorization of textile wastewater. Processes 8(1): 5.

Sonin D, Pochkaeva E, Zhuravskii S, Postnov V, Korolev D, Vasina L, Kostina D, Mukhametdinova D, Zelinskaya I and Skorik Y. (2020) Biological Safety and biodistribution of chitosan nanoparticles. Nanomaterials 10: 810.

Sreeja S and Nair CK. (2018) Tumor control by hypoxia-specific chemotargeting of iron-oxide nanoparticle–Berberine complexes in a mouse model. Life Sci. 195: 71-80.

Sun Y, Xu L, Zhang F, Song Z, Hu Y, Ji Y, Shen J, Li B, Lu H and Yang H. (2017) A promising magnetic sers immunosensor for sensitive detection of avian influenza virus. Biosens Bioelectron 89: 906-912.

Tamara FR, Lin C, Mi FL and Ho YC. (2018) Antibacterial effects of chitosan/cationic peptide nanoparticles. Nanomaterials 8(2): 88.

Üzek R, Sari E and Merkoçi A. (2019) Optical-based (bio) sensing systems using magnetic nanoparticles. Magnetochem. 5(4): 59.

Vaseashta AK and Mihailescu IN. (2008) Functionalized Nanoscale Materials, Devices and Systems; Springer Science Business Media: Dordrecht, The Netherlands, ISBN 978-1-4020-8903-9.

Villamin ME and Yoshitaka K. (2021) Facile synthesis and AC characterization of chitosan and iron oxide nanoparticles magnetic beads. AIP Conference Proc. https://doi.org/10.1063/1.5089449.

Yarjanli Z, Ghaedi K, Esmaeili A, Rahgozar S and Zarrabi A. (2017) Iron oxide nanoparticles may damage to the neural tissue through iron accumulation, oxidative stress, and protein aggregation. BMC Neurosci. 18(1): 1-12.

Zeinali S, Nasirimoghaddam S and Sabbaghi S. (2016) Investigation of the synthesis of chitosan coated iron oxide nanoparticles under different experimental conditions. Int J Nanosci Nanotechnol. 12(3):183-190.

Zhai Y, Feng H and Fu Y. (2022) A progressive online external parameter calibration and initialization method for stereo-IMU system. Industrial Robot 49(2): 344-358.

Zheng D, Zhang K, Gao K, Liu Z, Zhang X, Li O, Sun J, Zhang X, Du F, Sun P, Qu A and Wu X. (2013) Construction of novel *Saccharomyces cerevisiae* strains for bioethanol active dry yeast (ADY) production. PLoS ONE 8(12): e85022.

Zhu Y, Wang D, Wang F, Li T, Dong L, Liu H, Ma Y, Jiang F, Yin H, Yan W, Luo M, Tang Z, Zhang G, Wang Q, Zhang J, Zhou J and Yu J. (2013) A comprehensive analysis of GATA-1-regulated miRNAs reveals miR-23a to be a positive modulator of erythropoiesis. Nucleic Acids Res. 41(7): 4129-4143.

.